Sensors & Diagnostics

COMMUNICATION

View Article Online
View Journal | View Issue



Cite this: *Sens. Diagn.*, 2025, **4**, 574

Received 18th February 2025,
Accepted 12th April 2025

DOI: 10.1039/d5sd00023h

rsc.li/sensors

# A novel two-photon fluorescent probe for non-destructive imaging of $Hg^{2+}$ in fresh plant tissues†

Xiao Liu,‡[a] Zheng Zhu,‡[b] Ruitao Sun,[a] Jun Li*[a] and Shengzhen Xu *[a]

**In this work, we developed a small-molecule fluorescent probe (termed as LJTP3) for the specific detection of $Hg^{2+}$ with high sensitivity in living plant tissues. LJTP3 can not only effectively indicate the spatiotemporal distribution of $Hg^{2+}$ in the plant subcellular level, but also enable to realize 3D imaging of $Hg^{2+}$ in plant roots.**

Mercury, a highly toxic heavy metal, is widely distributed in the natural environment. However, with the increasing intensity of human activities such as industrial production, coal combustion, waste incineration and agricultural practices, mercury emissions have risen significantly, leading to serious environmental contamination.[1,2] As a major form of Hg, $Hg^{2+}$ exhibited a strong affinity for proteins with bioaccumulation properties.[3] As a critical component of ecosystems, plants are particularly sensitive to mercury pollution.[4] Studies have shown that $Hg^{2+}$ tends to accumulate in plant roots and leaves, and elevated levels can cause visible damage to plant tissues and further affect plant growth and crop production.[5,6] Therefore, developing an efficient tool for the detection of $Hg^{2+}$ in plants has great significance for agricultural management.

During the past decades, various traditional methods for detecting $Hg^{2+}$ have been developed, including but not limited to inductively coupled plasma atomic emission spectrometry (ICP-AES), inductively coupled plasma mass spectrometry (ICP-MS), atomic fluorescence spectrometry (AFS), atomic absorption spectrometry (AAS), and chemiluminescence methods.[7–10] Compared to these techniques, fluorescence sensors displayed distinct advantages, such as high sensitivity, superior spatiotemporal resolution, and non-invasive *in situ* imaging capabilities.[11–15] As a result, several fluorescent probes have been employed for the *in vivo* detection of $Hg^{2+}$.[16–21] However, only a few small-molecule organic fluorescent probes have been reported to achieve clear imaging at subcellular levels in plants.[22–28] In particular, two-photon fluorescent probes possess NIR excitation wavelengths, enabling deeper penetration into plant tissues to achieve plant subcellular imaging with minimum interference of background. However, two-photon-based small-molecule probes for subcellular imaging in plants are still few, and the dynamic distribution of $Hg^{2+}$ at subcellular lever still needs to be further investigated.[29–32]

In this study, a water-soluble fluorescent probe, **LJTP3** was tailored for the detection and imaging of $Hg^{2+}$ in plant tissues. It comprises a 2-(naphthalen-2-yl)benzo[*d*]oxazole-based fluorophore for signal output, and a hydrophilic tetrakis(*N*-2-hydroxyethyl)acetamide group as the $Hg^{2+}$ specific binding component. **LJTP3** exhibited not only excellent selectivity but also a low detection limit (LOD) of 0.08 μM for the early detection of $Hg^{2+}$. Moreover, the

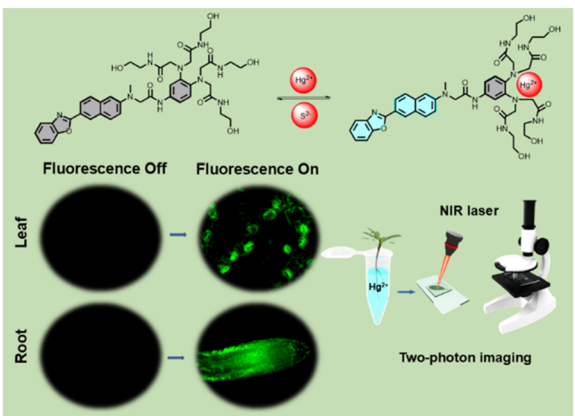


**Scheme 1** Illustration of a two-photon fluorescent probe (**LJTP3**) for the detection of $Hg^{2+}$ in *Arabidopsis thaliana*.

[a] *College of Chemistry, Huazhong Agricultural University, Wuhan, Hubei 430070, China. E-mail: xusz@mail.hzau.edu.cn*
[b] *College of Life Science and Technology, Huazhong Agricultural University, Wuhan, Hubei 430070, China*

† Electronic supplementary information (ESI) available. See DOI: https://doi.org/10.1039/d5sd00023h

‡ X. Liu and Z. Zhu contributed equally to this work.

fluorescence signals for $Hg^{2+}$ detection were observed in the model plant Arabidopsis, allowing visualization of its localization at the subcellular level. More importantly, the temporal and spatiotemporal distribution of mercury (Hg) was clearly observed under two-photon microscopy and 3D reconstruction (Scheme 1).

The synthetic procedures of **LJTP3** are shown in Scheme S1 (ESI†) and the molecular characterization data are shown in Fig. S1–S17 (ESI†). The synthesis of **LJTP3** was ultimately achieved through an 8-step process involving nucleophilic substitution, nitration, reduction, and condensation reactions to get the probe with moderate yields.

Following the successful synthesis of **LJTP3**, evaluation of its response to $Hg^{2+}$ was then performed in HEPES solution. As shown in Fig. S18 (ESI†), the probe itself has an obvious UV absorption peak at 355 nm in HEPES solution, which was employed as the excitation wavelength of **LJTP3**. The fluorescence titration experiment of **LJTP3** revealed that only $Hg^{2+}$ induced significant fluorescence enhancement at the emission peak of 480 nm, while other metal ions including $Ag^{+}$, $Ba^{2+}$, $Ca^{2+}$, $Cr^{3+}$, $Cd^{2+}$, $Fe^{2+}$, $Fe^{3+}$, $Mg^{2+}$, $Mn^{2+}$, $Na^{+}$, $Pd^{2+}$, and $Zn^{2+}$ did not induce obvious fluorescence enhancement, indicating the good selectivity of **LJTP3** (Fig. 1A). In addition, fluorescence interference tests for different ions were carried out in HEPES solution. As shown in Fig. 1B, the fluorescence of the probe **LJTP3** shows minimal interference from other coexisting metal ions, demonstrating its strong anti-interference capability. This suggests that **LJTP3** can be well-suited for the selective detection of $Hg^{2+}$ in complex systems. The fluorescence spectra of the probe **LJTP3** (1 μM) were measured at varying concentrations of $Hg^{2+}$ (0–10 μM), as shown in Fig. 1C. The fluorescence intensity gradually increased with increasing $Hg^{2+}$ concentrations, until reaching a plateau. During the titration experiments, a good linear relationship was observed between the fluorescence intensity and concentrations of $Hg^{2+}$ in the range of 0–3 μM (Fig. 1D). The limit of detection (LOD) was determined to be 0.08 μM.

The binding mode of the probe **LJTP3** for $Hg^{2+}$ was hypothesized, as shown in the Fig. S19.† Upon coordination of the polyamide ligands with $Hg^{2+}$, the PET effect was weakened, leading to enhance fluorescence intensity. To confirm this hypothesis, the detection mechanism of **LJTP3** toward $Hg^{2+}$ was thoroughly validated using ESI-MS. As shown in Fig. S20 (ESI†), the molecular ion peak (*m*/*z*: 1044.3536) was observed, which matches the calculated value (*m*/*z*: 1044.3538).

Additionally, a Job-plot experiment was conducted (Fig. 1F). The intersection of the curve at a ratio of 0.5 indicates a 1 : 1 binding ratio between **LJTP3** and $Hg^{2+}$. Due to its specific affinity for $S^{2-}$, the $Hg^{2+}$-enhanced fluorescence was restored to the level of the free probe. This rapid and reversible sensing behavior was repeated five times without significant signal attenuation (Fig. 1E), confirming the reversibility of the binding. Besides, **LJTP3** exhibited high stability within the pH range of 6.5–8.0, making it suitable for $Hg^{2+}$ sensing under physiological conditions (Fig. S21 ESI†).

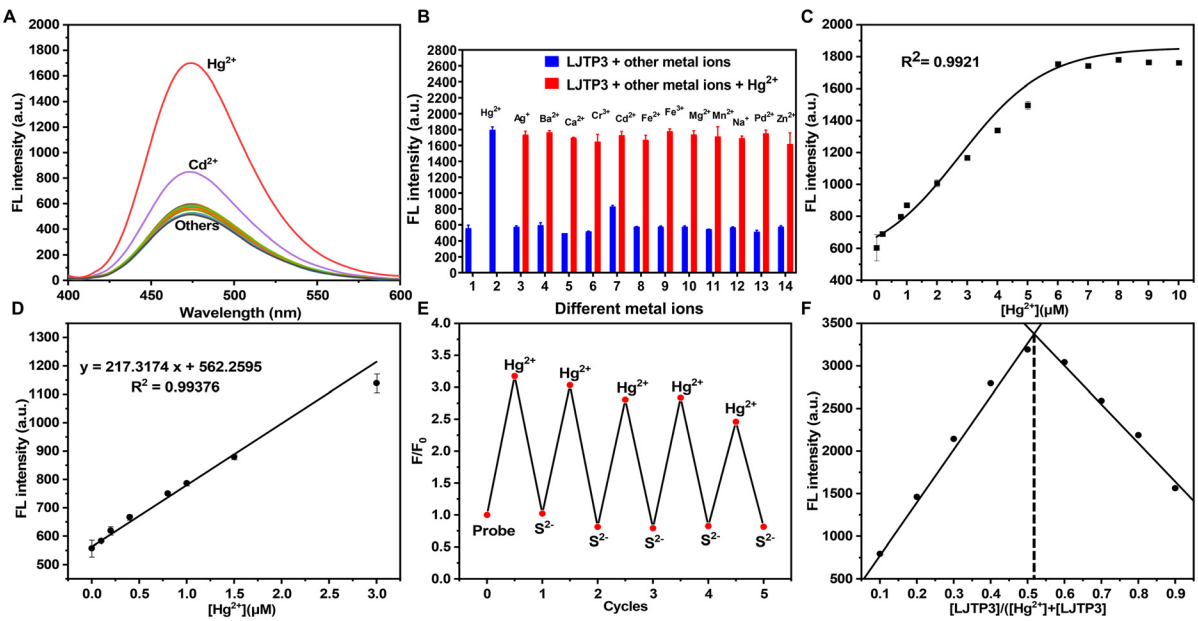


**Fig. 1** (A) Fluorescence response of **LJTP3** (1 μM) towards various metal ions (10 μM), including $Hg^{2+}$, $Ag^{+}$, $Ba^{2+}$, $Ca^{2+}$, $Cr^{3+}$, $Cd^{2+}$, $Fe^{2+}$, $Fe^{3+}$, $Mg^{2+}$, $Mn^{2+}$, $Na^{+}$, $Pd^{2+}$, and $Zn^{2+}$. (B) Fluorescence selectivity of **LJTP3** (1 μM) with $Hg^{2+}$ (10 μM) in the presence of various metal ions (10 μM), including 1. the probe only, 2. $Hg^{2+}$, 3. $Ag^{+}$, 4. $Ba^{2+}$, 5. $Ca^{2+}$, 6. $Cr^{3+}$, 7. $Cd^{2+}$, 8. $Fe^{2+}$, 9. $Fe^{3+}$, 10. $Mg^{2+}$, 11. $Mn^{2+}$, 12. $Na^{+}$, 13. $Pd^{2+}$, and 14. $Zn^{2+}$. (C) Fluorescence titration of **LJTP3** (1 μM) with different concentrations of $Hg^{2+}$. (D) Linear relationship of **LJTP3** with different concentrations of $Hg^{2+}$ in the range of 0–3.0 μM. (E) Fluorescence response of **LJTP3** based on emission at 480 nm in cycles of $Hg^{2+}$ (1 μM) addition and subsequent $Na_2S$ (1 μM) treatment. (F) Job-plots of the fluorescence intensity of **LJTP3**.

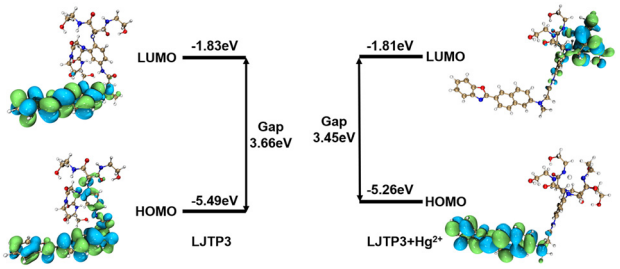


Fig. 2 Molecular orbitals and corresponding energy levels of **LJTP3** and **LJTP3** + $Hg^{2+}$ in both the ground state and excitation state.

To investigate the sensing mechanism (Fig. 2), density functional theory (DFT) calculations were performed using Gaussian 16 software.[33] The highest occupied molecular orbital (HOMO) and lowest unoccupied molecular orbital (LUMO) of **LJTP3** were primarily localized on the fluorophore, although the HOMO also exhibited partial distribution in the recognition group. The energy gap between the HOMO and LUMO was calculated to be 3.66 eV, with photo-induced electron transfer (PET) occurring from the recognition group to the fluorophore, resulting in fluorescence quenching. Upon binding with $Hg^{2+}$, the distribution of both the HOMO and LUMO shifted towards the fluorophore and recognition group, respectively, with a reduced energy gap of 3.45 eV, leading to the inhibition of PET and consequently, fluorescence restoration.

Given the advantages of two-photon microscopy, we employed this technique to further verify the probe's efficiency in detecting $Hg^{2+}$ at the tissue and cellular level. To evaluate the probe's specificity *in vivo* (Fig. 3A and B), the model plant *Arabidopsis thaliana* was treated with various metal ions including $Cd^{2+}$, $Mg^{2+}$, $Zn^{2+}$, $K^{+}$ and $Hg^{2+}$ respectively and then imaged under two-photon microscopy ($\lambda_{ex}$ = 750 nm);[34] only the $Hg^{2+}$ treated group showed significant fluorescence signal output, indicating **LJTP3** can be employed for $Hg^{2+}$ specific imaging in plant tissues. As evidenced in Fig. S23,† two-photon comparative experiments were systematically conducted to examine the system before and after $S^{2-}$ introduction. The experimental data demonstrate near-complete fluorescence quenching upon $S^{2-}$ addition, strongly suggesting the reversible binding behavior between **LJTP3** and $Hg^{2+}$ in plant systems. In addition, the translocation of $Hg^{2+}$ in plant tissues at the subcellular level, as well as the stress response of plant cells under $Hg^{2+}$ exposure, were visualized in a real time manner (Fig. 3D and E). In the control group, where $Hg^{2+}$ was absent, only a faint fluorescence signal was detected. However, after 1 hour of incubation with $Hg^{2+}$, fluorescence corresponding to the probe's interaction with $Hg^{2+}$ appeared on the epidermal cells of the root tip. After 3 hours, the fluorescence became more widespread, reflecting a significant uptake of the probe within the root tip cells. Moreover, after 5 hours, the fluorescence intensity increased markedly, indicating a strong and clear signal. Similar trends were observed in the Arabidopsis leaf epidermis (Fig. S21C and D ESI†).

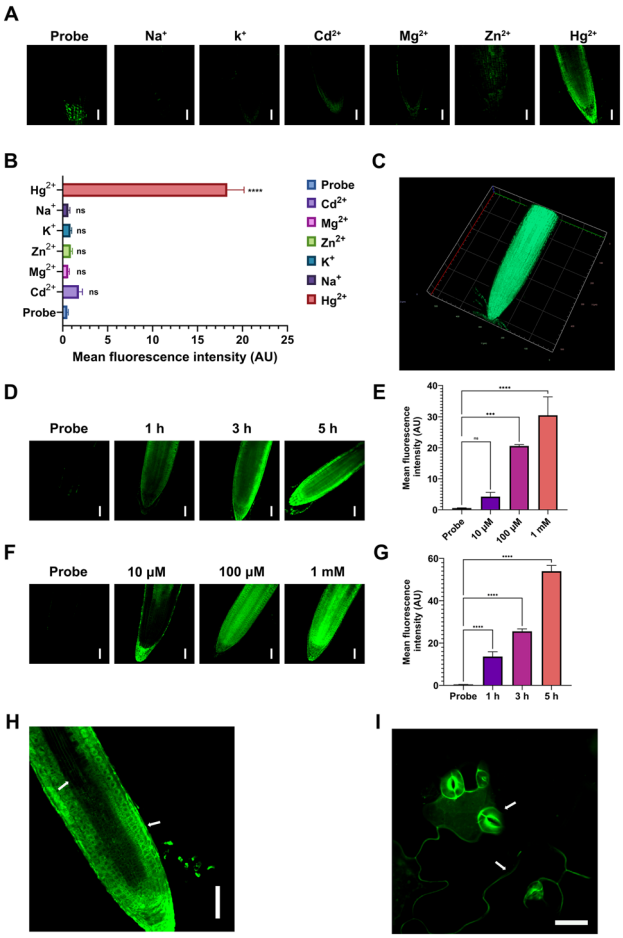


Fig. 3 *In vivo* imaging of $Hg^{2+}$ with **LJPT3**. (A and B) Elemental selective imaging fluorescence pictures of **LJPT3** and their quantitative data. (C) 3D reconstruction of **LJPT3** signal distribution in plant roots. (D and E) Fluorescence pictures of Arabidopsis root tips under different $Hg^{2+}$ treatment times and their quantitative data. (F and G) Fluorescence pictures of Arabidopsis root tips treated with different concentrations of $Hg^{2+}$ and their quantitative data. (H) Fine structure imaging fluorescence picture of Arabidopsis root tips. (I) Fine structure imaging fluorescence picture of Arabidopsis leaf epidermis (scale bar = 50 μm).

To further investigate the fluorescence signal transmission in Arabidopsis under different $Hg^{2+}$ concentrations, two-photon imaging was performed on root tips under varying $Hg^{2+}$ stress levels (Fig. 3F and G). Only weak fluorescence signals were detected in the control group (no $Hg^{2+}$ treatment). Under the stress of 10 μM $Hg^{2+}$, fluorescence signals began to appear around the cells of Arabidopsis root tips. At 100 μM $Hg^{2+}$, signals are present in most cells of the root tip. When the concentration was increased to 1 mM, signals appeared in all cells of the root tip and exhibited very high fluorescence intensity. In the leaf epidermis under the same treatment, the signal changed in a similar trend (Fig. S21A and B ESI†). The above results manifested that the dynamic distribution of $Hg^{2+}$ can be visualized using **LJTP3**.

Under a single photon microscope with 3D imaging and reconstruction, **LJPT3** can also directly visualize the spatial

distribution of $Hg^{2+}$ in plant organs (Fig. 3C). In summary, **LJPT3** can realize the non-destructive detection of $Hg^{2+}$ in plant organs and tissues in a very short time, with good selectivity and sensitivity, and can accurately indicate the location and content of $Hg^{2+}$ in plants.

To evaluate the capability of **LJPT3** in detecting $Hg^{2+}$ distribution differences within plant tissue microstructures, fluorescence signals in Arabidopsis root tips and leaf epidermis were analyzed using two-photon microscopy. Under 10 μM $Hg^{2+}$ treatment, the root epidermis exhibited stronger fluorescence than the stele, reflecting a defense strategy against mercury. Likewise, the leaf epidermis showed higher fluorescence than the root stele, indicating differential $Hg^{2+}$ accumulation (Fig. 3H), consistent with previous reports.

This disparity is attributed to plant cell defense mechanisms against $Hg^{2+}$, aligning with previous findings.[35] In leaves, stomata exhibited stronger fluorescence than epidermal cells (Fig. 3I), as they serve as key sites for $Hg^{2+}$ exchange between plants and the environment. Plants absorb elemental mercury *via* the stomata and convert accumulated mercury in leaves into elemental form for release.[36]

In conclusion, we have designed a highly efficient fluorescent probe (**LJTP3**) specifically to study $Hg^{2+}$ stress in plant tissues. **LJTP3** demonstrated excellent selectivity and sensitivity for the early detection of $Hg^{2+}$ in aqueous solution, with a detection limit of 0.08 μM. Remarkably, **LJTP3** exhibited outstanding selectivity for $Hg^{2+}$ in both *in vitro* tests and plant imaging. Moreover, under two-photon imaging, the distribution of $Hg^{2+}$, along with $Hg^{2+}$-induced rupture of root tip cells and leaf stomata, was clearly observed. We believe that this study not only provides a novel imaging tool for investigating $Hg^{2+}$-induced stress on plant cell structures but also contributes to the management of Hg pollution in agriculture.

## Data availability

The authors confirm that the data supporting the findings of this study are available within the article and its ESI.†

## Author contributions

Shengzhen Xu and Jun Li conceived the basic idea and reviewed the manuscript. Xiao Liu designed and performed the experiment and drafted the manuscript. Zheng Zhu performed the experiments and imaging; Ruitao Sun provided suggestions on experiment. All authors read and approved the manuscript. Xiao Liu and Zheng Zhu contributed equally to this work.

## Conflicts of interest

There are no conflicts to declare.

## Acknowledgements

This work was financially supported by the Minhui Cao Studio of Huazhong Agricultural University.

## Notes and references

1 C. T. Driscoll, R. P. Mason, H. M. Chan, D. J. Jacob and N. Pirrone, *Environ. Sci. Technol.*, 2013, **47**, 4967–4983.
2 Y. S. Wu, A. I. Osman, M. Hosny, A. M. Elgarahy, A. S. Eltaweil, D. W. Rooney, Z. H. Chen, N. S. Rahim, M. Sekar, S. C. B. Gopinath, N. N. I. M. Rani, K. Batumalaie and P. S. Yap, *ACS Omega*, 2024, **9**, 5100–5126.
3 P. A. Nogara, C. S. Oliveira, G. L. Schmitz, P. C. Piquini, M. Farina, M. Aschner and B. T. Rocha, *Biochim. Biophys. Acta, Gen. Subj.*, 2019, **1863**, 129–284.
4 B. Gworek, W. Dmuchowski and A. H. Baczewska-Dąbrowsk, *Environ. Sci. Eur.*, 2020, **32**, 128.
5 J. Zhou, D. Obrist, A. Dastoor, M. Jiskra and A. Ryjkov, *Nat. Rev. Earth Environ.*, 2021, **2**, 269284.
6 W. Yuan, X. Wang, C. J. Lin, F. Wu, K. Luo, H. Zhang, Z. Y. Lu and X. B. Feng, *Environ. Sci. Technol.*, 2022, **56**, 14154–14165.
7 S. Li, C. C. Zhang, S. N. Wang, Q. Liu, H. H. Feng, X. Ma and J. H. Guo, *Analyst*, 2018, **143**, 4230–4246.
8 T. A. Saleh, G. Fadillah, E. Ciptawati and M. Khaled, *TrAC, Trends Anal. Chem.*, 2020, **132**, 116016.
9 K. Schlöglova, M. Wälle and C. A. Heinrich, *J. Anal. At. Spectrom.*, 2017, **32**, 1052–1063.
10 K. Srinivasan, K. Subramanian, A. Rajasekar, K. Murugan, G. Benelli and K. Dinakaran, *Bull. Mater. Sci.*, 2017, **40**, 1455–1462.
11 M. C. Dai, Y. J. Yang, S. Sarkar and K. H. Ahn, *Chem. Soc. Rev.*, 2023, **52**, 6344–6358.
12 X. L. Ding, Q. Wang, D. Chen, Y. L. Chen, W. W. Pan, Q. Sun, Q. Chen and X. Y. Han, *Adv. Agrochem*, 2023, **2**, 364–370.
13 J. Yin, Y. Hu and J. Y. Yoon, *Chem. Soc. Rev.*, 2015, **44**, 4619–4644.
14 Z. J. Zhang, B. R. Adhikari, P. Sen, L. Soleymani and Y. F. Li, *Adv. Agrochem*, 2023, **2**, 246–257.
15 J. Li, D. Yim, W.-D. Jang and J. Yoon, *Chem. Soc. Rev.*, 2017, **46**, 2437–2458.
16 L. H. Feng, Y. Deng, X. J. Wang and M. G. Liu, *Sens. Actuators, B*, 2017, **245**, 441–447.
17 G. J. Li, J. L. Wang, D. Y. Li, S. H. Liu, J. Yin, Z. B. Lai and G. F. Yang, *Chin. Chem. Lett.*, 2021, **32**, 1527–1531.
18 J. H. Wang, Y. M. Liu, Z. M. Dong, J. B. Chao, H. Wang, Y. Wang and S. M. Shuang, *J. Hazard. Mater.*, 2020, **382**, 121056.
19 L. N. Neupane, J. Park, P. K. Mehta, E. T. Oh, H. J. Park and K. H. Lee, *Chem. Commun.*, 2020, **56**, 2941–2944.
20 Z. G. Wang, Y. Zhang, J. Yin, Y. Q. Yang, H. Luo, J. Song, X. Xu and S. F. Wang, *ACS Sustainable Chem. Eng.*, 2020, **33**, 12348–12359.
21 L. Wang, Y. Ma and W. Y. Lin, *J. Hazard. Mater.*, 2024, **461**, 132604.

22 Y. Y. Zhang, W. Shi, D. Feng, H. M. Ma, Y. Liang and J. R. Zuo, *Sens. Actuators, B*, 2011, **153**, 261–265.
23 Y. Yang, R. Shen, Y. Z. Wang, F. Z. Qiu, Y. Feng, X. L. Tang, D. C. Bai, G. L. Zhang and W. S. Liu, *Sens. Actuators, B*, 2018, **255**, 3479–3487.
24 K. Ramki, G. Thiruppathi, S. K. Ramasamy, P. Sundararaj and P. Sakthivel, *Methods*, 2024, **221**, 1–11.
25 H. Y. Niu, T. Q. Ye, L. Y. Yao, Y. F. Lin, K. Chen, Y. B. Zeng, L. Li, L. H. Guo and J. B. Wang, *J. Hazard. Mater.*, 2024, **475**, 134914.
26 Y. An, B. Li, Y. Z. Yu, Y. C. Zhou, J. F. Yi, L. P. Li, Y. Q. Sun, Z. Z. Qiang, Y. Q. Liu and P. Wang, *J. Hazard. Mater.*, 2024, **465**, 133331.
27 C. Zhao, A. Aziz, W. J. Lu, H. M. Xu, M. Asif, S. M. Shuang and C. Dong, *J. Hazard. Mater.*, 2024, **479**, 135694.
28 J. H. Wang, Y. M. Liu, Z. M. Dong, J. B. Chao, H. Wang, Y. Wang and S. M. Shuang, *J. Hazard. Mater.*, 2020, **382**, 121056.
29 J. Z. Du, K. M. Chen, Z. Y. Yu, Y. H. Qiao, J. X. Liu, Q. Q. Zhai, Z. Hu, S. G. Yang, J. Li and H. L. Teng, *Adv. Agrochem*, 2022, **1**, 162–173.
30 V. Juvekar, S. J. Park, J. Y. Yoon and H. M. Kim, *Coord. Chem. Rev.*, 2021, **427**, 213574.
31 H. W. Lee, V. Juvekar, D. J. Lee and H. M. Kim, *TrAC, Trends Anal. Chem.*, 2023, **165**, 117128.
32 S. Asghar, Z. Yu, Z. Zhu, D. Zheng, Z. Zhao, Y. Xu, X. Liu, C. Yuan, Y. Li, W. Wang, J. F. Xu, H. L. Teng, J. Li, W. C. Yang and C. Chen, *Research*, 2025, **8**, 0570.
33 G. J. Li, J. L. Wang, D. Y. Li, S. H. Liu, J. Yin, Z. B. Lai and G. F. Yan, *Chin. Chem. Lett.*, 2021, **32**, 1527–1531.
34 H. J. Kim, J. H. Han, M. K. Kim, C. S. Lim, H. M. Kim and B. R. Cho, *Angew. Chem.*, 2010, **122**, 6938–6941.
35 J. J. Wang, Y. Y. Guo, D. L. Guo, S. L. Yin, D. L. Kong, Y. S. Liu and H. Zeng, *Environ. Sci. Technol.*, 2012, **46**, 769–777.
36 W. Yuan, X. Wang, C. J. Lin, F. Wu, K. Luo, H. Zhang, Z. Y. Lu and X. B. Feng, *Environ. Sci. Technol.*, 2022, **56**, 14154–14165.